

THE FORMATION OF ICE GIANTS IN A PACKED OLIGARCHY:  
INSTABILITY AND AFTERMATHERIC B. FORD<sup>1,2</sup> AND EUGENE I. CHIANG<sup>3,4</sup>INCORPORATES REFEREE'S COMMENTS: *Jan 25, 2007*

## ABSTRACT

As many as 5 ice giants—Neptune-mass planets composed of  $\sim 90\%$  ice and rock and  $\sim 10\%$  hydrogen—are thought to form at heliocentric distances of  $\sim 10$ – $25$  AU on closely packed orbits spaced  $\sim 5$  Hill radii apart. Such oligarchies are ultimately unstable. Once the parent disk of planetesimals is sufficiently depleted, oligarchs perturb one another onto crossing orbits. We explore both the onset and the outcome of the instability through numerical integrations, including dynamical friction cooling of planets by a planetesimal disk whose properties are held fixed. To trigger instability and the ejection of the first ice giant in systems having an original surface density in oligarchs of  $\Sigma \sim 1 \text{ g/cm}^2$ , the disk surface density  $\sigma$  must fall below  $\sim 0.1 \text{ g/cm}^2$ . Ejections are predominantly by Jupiter and occur within  $\sim 10^7 \text{ yr}$ . To eject more than 1 oligarch requires  $\sigma \lesssim 0.03 \text{ g/cm}^2$ . For certain choices of  $\sigma$  and initial semi-major axes of planets, systems starting with up to 4 oligarchs in addition to Jupiter and Saturn can readily yield solar-system-like outcomes in which 2 surviving ice giants lie inside 30 AU and have their orbits circularized by dynamical friction. Our findings support the idea that planetary systems begin in more crowded and compact configurations, like those of shear-dominated oligarchies. In contrast to previous studies, we identify  $\sigma \lesssim 0.1\Sigma$  as the regime relevant for understanding the evolution of the outer solar system, and we encourage future studies to concentrate on this regime while relaxing our assumption of a fixed planetesimal disk. Whether evidence of the instability can be found in Kuiper belt objects (KBOs) is unclear, since in none of our simulations do marauding oligarchs excite as large a proportion of KBOs having inclinations  $\gtrsim 20^\circ$  as is observed.

*Subject headings:* celestial mechanics—Kuiper belt—planets and satellites : formation—solar system : formation

## 1. INTRODUCTION

Without gravitational focussing, *in situ* coagulation of Uranus and Neptune takes too long to complete. In a minimum-mass disk at heliocentric distances of 20–30 AU, timescales to assemble the ice giants exceed the age of the solar system by 2 orders of magnitude, if growth is unfocussed (e.g., Goldreich, Lithwick, & Sari 2004, hereafter GLS04).<sup>5</sup> N-body coagulation simulations that do not damp relative velocities between planetesimals, either by dynamical friction, inelastic collisions, or gas drag, fail to form Uranus and Neptune (Levison & Stewart 2001; see also Lissauer et al. 1995). The ice giants contain 10–20% hydrogen by mass, a fraction so large that such gas must originate from the solar nebula. The outer planets must therefore form within a few  $\times 10^7 \text{ yr}$ , before all of the nebular hydrogen photoevaporates (Shu, Johnstone, & Hollenbach 1993; Matsuyama, Johnstone, & Hartmann 2003).

One way to alleviate (but not necessarily eliminate) the timescale problem is to form Uranus and Neptune closer to the Sun, where material densities and collision

rates are greater. Thommes, Levison, & Duncan (1999, 2002) explore a scenario in which the two planets form at distances of 5–10 AU, between the cores of Jupiter and Saturn. Once the gas giant cores amass their envelopes, they scatter the ice giants outward onto eccentric orbits. These orbits subsequently circularize by dynamical friction with planetesimals at 15–30 AU. Tsiganis et al. (2005) propose an alternative history in which Uranus and Neptune accrete at 12 and 17 AU, are thrown outward by Jupiter and Saturn, and have their orbits circularized by dynamical friction. According to their story, the outward scattering of ice giants is triggered by having Jupiter and Saturn divergently migrate across their mutual 2:1 resonance.

Another approach to solving the timescale problem is to consider how gravitational focussing can be amplified. GLS04 adopt this route by appealing to a massive disk of sub-km-sized planetesimals, similar to those produced by coagulation simulations set in the outer solar system (Kenyon & Luu 1999). The disk envisioned by GLS04 has a mass several times the minimum-mass value in condensates so that the “isolation mass”—the mass to which a protoplanet grows by consuming all material within its annulus of influence—equals Neptune’s mass. The small bodies comprising the disk collide so frequently that their velocity dispersion damps to values less than the Hill velocity of a Neptune-mass planet. Accretion rates then enjoy maximal enhancement by gravitational focussing, and proto-Neptune can accrete the last half of its mass in  $\sim 10^5 \text{ yr}$  (see eqn. 105 of GLS04). Gas drag supplies another means to damp planetesimal velocity dispersions (Rafikov 2004; Chambers 2006; see also appendix A of

Electronic address: [eford@cfa.harvard.edu](mailto:eford@cfa.harvard.edu), [echiang@astron.berkeley.edu](mailto:echiang@astron.berkeley.edu)<sup>1</sup> Harvard-Smithsonian Center for Astrophysics, Mail Stop 51, 60 Garden Street, Cambridge, MA 02138, USA<sup>2</sup> Hubble Fellow<sup>3</sup> Center for Integrative Planetary Sciences, Astronomy Department, University of California at Berkeley, Berkeley, CA 94720, USA<sup>4</sup> Alfred P. Sloan Research Fellow<sup>5</sup> The problem does not disappear by merely raising the disk mass above the minimum-mass value, since the gravitationally unfocussed growth rate scales only linearly with the disk surface density.

GLS04).

Strongly focussed, *in situ* assembly of planets from a dynamically cold disk carries, however, a potential embarrassment of riches: The disk can spawn more ice giants than the solar system's current allotment of 2 (Uranus and Neptune). We estimate that about 5 isolation masses or “oligarchs,” each having the mass of Neptune, can form between 15 and 25 AU (see eqn. 1 below). These planets comprise a “shear-dominated oligarchy,” so-called because the encounter velocities between planets and planetesimals are given by their minimum values set by Keplerian shear. Initially, the oligarchs' nested orbits would be stabilized by dynamical friction with the disk. GLS04 suggest that excess oligarchs would be purged from the outer solar system by an eventual dynamical instability. According to their order-of-magnitude analysis, this “velocity instability” occurs once the mass of the disk becomes less than the mass in oligarchs, whereupon dynamical friction ceases to stabilize the system against mutual gravitational stirring (a.k.a. “viscous stirring”). In the ensuing chaos, several oligarchs would be ejected, either by other oligarchs or by Jupiter or Saturn, possibly leaving two survivors whose orbits could circularize by dynamical friction at 15–30 AU.

Despite their disparate perspectives on the timescale problem and different motivations, the scenarios of Thommes et al. (1999), Tsiganis et al. (2005), and GLS04 share quite a few features. In their simplest forms, each theory starts with a more crowded configuration for solar system planets than is observed today; each is characterized by an intermediate period of dynamical chaos during which Uranus and Neptune execute highly eccentric orbits; and each invokes final regularization of ice giant orbits by dynamical friction with an ambient disk. Thommes et al. (2002) and Chiang et al. (2006, hereafter C06) point out that these violent histories might be encoded in Kuiper belt objects (KBOs). In particular, so-called scattered KBOs possess large eccentricities, inclinations, and perihelion distances which might reflect gravitational stirring by marauding ice giants.

The notion that planets originate in compact and crowded configurations is bolstered by the study of extra-solar systems as well. To explain the striking preponderance of large orbital eccentricities observed among extra-solar giant planets (Butler et al. 2006), multiple planets each having on the order of a Jupiter mass are imagined to have once resided on orbits sufficiently close that the planets scatter one another onto elliptical trajectories (Marzari & Weidenschilling 2002; Ford, Rasio, & Yu 2003; Ford, Lystad, & Rasio 2005).

GLS04 outline a possible formation history for Uranus and Neptune in a packed oligarchy, and C06 expand upon its consequences for the Kuiper belt, by making many simplifying assumptions and order-of-magnitude approximations. In this paper, we test some of their ideas by numerical simulations. In particular, we seek answers to the following questions:

1. For a shear-dominated oligarchy containing more than two Neptune-mass oligarchs beyond Saturn's orbit, what is the critical value of the disk surface density below which the velocity instability occurs?
2. What is the likelihood that the instability will re-

sult in the survival of two oligarchs whose final orbits resemble those of Uranus and Neptune?

3. To what degree is the Kuiper belt dynamically excited by velocity-unstable oligarchs?

Our methods are described and tested in §2. That section contains empirical determinations of how rapidly 5 oligarchs viscously stir one another, with and without the gas giants Jupiter and Saturn. Comparisons are made with analytic theory. Results of hundreds of simulations designed to provide statistical answers to the above questions are presented in §3. We summarize and offer an outlook in §4.

## 2. METHOD AND TESTS

To guide the reader, we provide a condensed description of our method in §2.1. Details are elaborated upon in §§2.2–2.3.

### 2.1. Overview

We simulate the final stages of oligarchy by numerically integrating the trajectories of 5 closely packed Neptune-mass oligarchs, together with those of 2 gas giants resembling Jupiter and Saturn. Oligarchs and gas giants are referred to as planets. We employ the hybrid orbit integrator MERCURY6 (Chambers 1999), which combines a conventional Bulirsch-Stoer integrator to handle close encounters between planets, with the fast symplectic algorithm invented by Wisdom & Holman (1991). Viscous stirring of an oligarch by other planets is simulated as accurately as the orbit integrator solves the gravitational equations of motion. Case studies of viscous stirring are described in §2.2.

To model dynamical friction between a planet and the surrounding disk of planetesimals, we introduce a perturbative force on each planet. The force damps the component of the planet's velocity that differs from the local disk (circular) velocity. For simplicity, we take the disk to have a constant surface density between an inner and an outer radius. Disk parameters are held fixed. In our simple scheme, the planets respond to the disk through dynamical friction, but the disk does not respond to the planets. The details of the perturbation force are provided in §2.3. The validity of our fixed disk approach is briefly considered in §4.2.2.

Finally, to investigate how oligarchs might excite the Kuiper belt, an ensemble of test particles is included in a subset of the simulations. We use the terms “test particle” and “Kuiper belt object (KBO)” interchangeably. These test particles are intended to represent large KBOs like those observed today, having sizes on the order of 100 km. This size is small enough that we can neglect dynamical friction between KBOs and the disk, yet also large enough that we can ignore damping of KBOs' velocities by physical collisions with the disk (C06). Thus, in our simulations, KBOs (test particles) feel directly only the gravity of the Sun and of the planets.

In the sub-sections below, we explore separately the processes of viscous stirring (§2.2) and dynamical friction (§2.3), in isolation from one another. We present full-fledged simulations, in which the two processes are combined, in §3.

## 2.2. Viscous Stirring

We first study how multiple oligarchs gravitationally stir one another. For this sub-section, we ignore dynamical friction with the disk, but include the gas giants, Jupiter and Saturn. We compare our findings to those of GLS04. The results of this sub-section will be applied in §3 to understanding the threshold conditions required for velocity instability.

### 2.2.1. Initial Conditions

We consider  $N_{\text{olig}} = 5$  oligarchs, each having the mass of Neptune ( $\mu = m/m_{\odot} = m_{\text{N}}/m_{\odot} = 5.1 \times 10^{-5}$ ). The oligarchs are initially spaced 5 Hill radii apart in semi-major axis ( $a$ ); that is, the difference between semi-major axes of nearest-neighboring oligarchs is

$$a_{j+1} - a_j = 2.5(\mu/3)^{1/3}a_j + 2.5(\mu/3)^{1/3}a_{j+1}, \quad (1)$$

where  $j$  ranges from 1 to  $N_{\text{olig}}$ . The coefficient of 2.5 is inspired by numerical studies by Greenberg et al. (1991) of the width of a protoplanet’s feeding zone, for the case where Keplerian shear dominates the relative velocity between a protoplanet and a planetesimal (see their eqn. 9; see also Ida & Makino 1993). While the coefficient of 2.5 is the standard value for our study, the coefficient in reality can be somewhat different, depending on the accretion and migration histories of the planets. We explore some consequences of varying the coefficient in §2.2.3 and §4.2.4.

We assume the semi-major axis of the innermost oligarch  $a_1 = 15$  AU. Then according to eqn. (1), semi-major axes of the next four oligarchs equal 17.1, 19.4, 22.1, and 25.1 AU. Initial eccentricities, and initial inclinations relative to an arbitrary reference (x-y) plane, are such that  $e_j = \sin i_j = 10^{-4}$ . All orbital elements in this paper are osculating and referred to a barycentric coordinate system. That is, when computing the osculating Kepler elements for a given body, the position and velocity of the body are referred to the system barycenter (calculated using all massive bodies), while the central mass of the assumed Kepler potential equals the mass of the Sun plus that of the given body (alone). For each oligarch, the initial longitude of ascending node, longitude of pericenter, and mean anomaly are randomly generated from uniform distributions between 0 and  $2\pi$ .

Jupiter and Saturn are assigned initial masses and semi-major axes equal to their current values:  $\mu_J = m_J/m_{\odot} = 9.5 \times 10^{-4}$ ,  $\mu_S = m_S/m_{\odot} = 2.9 \times 10^{-4}$ ,  $a_J = 5.18$  AU, and  $a_S = 9.54$  AU. Initial eccentricities equal  $e_J = e_S = 0.05$ , and inclinations relative to the reference plane are such that  $\sin i_J = \sin i_S = 0.01$ . Orbital longitudes are randomly generated, just as they are for the oligarchs.

These initial conditions, particularly our choices for  $a_1 = 15$  AU and  $N_{\text{olig}} = 5$ , are somewhat arbitrary. They are intended to represent qualitatively the final stages of shear-dominated oligarchy in the outer solar system. We will adjust starting parameters (e.g.,  $a_1$ ,  $N_{\text{olig}}$ ) in later sections to achieve simulation outcomes in better agreement with observed properties of the solar system.

A total of  $N_{\text{real}} = 200$  orbital integrations (“realizations”) are performed with the hybrid integrator MERCURY6 (Chambers 1999), each characterized by a

unique set of starting longitudes and each lasting  $10^7$  yr. The timestep for the symplectic integrator is set to 130 days. Timesteps for the conventional Bulirsch-Stoer integrator are as short as necessary to achieve an accuracy parameter of  $10^{-10}$ . The changeover distance that separates the symplectic regime from the close encounter regime is set to  $\Delta r_{\text{crit}} = 3$  Hill radii.

A “collision” between two bodies occurs when their mutual separation becomes less than the sum of their physical radii. The physical radius of each oligarch is computed using Neptune’s bulk density of  $1.6 \text{ g/cm}^3$ . Physical radii for Jupiter and Saturn are computed using densities of  $1.3$  and  $0.7 \text{ g/cm}^3$ , respectively. We assume that bodies that collide merge completely.

An “ejection” occurs when an oligarch’s distance from the Sun exceeds 10000 AU and when its total kinetic plus potential energy (evaluated in barycentric coordinates with the potential energy set to zero at infinity) becomes positive. Ejected planets are dropped from the simulation.

### 2.2.2. Results: Outcomes After $t = 10^7$ yr

At  $t = 10^7$  yr, the outcomes for all  $N_{\text{all}} = N_{\text{real}} \times N_{\text{olig}} = 200 \times 5 = 1000$  oligarchs divide into the following mutually exclusive categories, in order of decreasing frequency of incidence:

1. Ejection but no collision (463)
2. No collision and no ejection (439)
3. Collision with another oligarch but no ejection (42; i.e., 21 oligarchs remain, each with mass twice that of an original oligarch)
4. Collision with Sun only (19)
5. Collision with Jupiter only (14)
6. Collision with another oligarch, and subsequent ejection or subsequent collision with Jupiter or Saturn (13)
7. Collision with Saturn only (10)

The dominant outcome is ejection. In 50% of the realizations (i.e., 100 out of  $N_{\text{real}} = 200$ ), at least one oligarch is ejected before  $t = 1.6 \times 10^6$  yr. By  $t = 3.2 \times 10^6$  yr, 85% of all realizations experience a first ejection. All but 5 out of 200 realizations experience at least one ejection of an oligarch by  $t = 10^7$  yr.

Jupiter and Saturn are responsible for the preponderance of ejections. When we repeat the experiment with Jupiter and Saturn omitted, outcomes at  $t = 10^7$  yr are as follows: 870 out of 1000 oligarchs experience neither an ejection nor a collision, 118 collide with another oligarch (so that 59 remain), and 12 collide with two other oligarchs (so that 4 remain). No ejection is observed to occur by  $t = 10^7$  yr when the gas giants are absent.

These outcomes are consistent with timescale estimates by GLS04. Neglecting Jupiter and Saturn, GLS04 predict that the oligarch ejection timescale is  $\sim 10^9$  yr (see their eqn. 114). This is consistent with our finding that no ejection occurs within  $t = 10^7$  yr in the absence of gas giants. GLS04 mention the possibility that Jupiter and Saturn hasten ejections. We confirm this possibility. When gas giants are present, we find the ejection timescale is  $\sim 10^6$  yr.

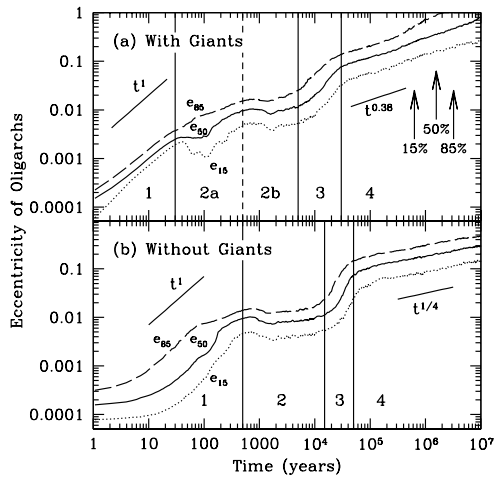


FIG. 1.— Viscous stirring of oligarchs, in the absence of dynamical friction, for an oligarch separation of  $5R_H$ . We show the median (solid curve), 85<sup>th</sup> percentile (long dashed curve), and 15<sup>th</sup> percentile (dotted curve) of the oligarchs' eccentricity distribution versus time, based on N-body integrations with no dynamical friction. In panel (a), each integration includes Jupiter, Saturn, and five oligarchs. In panel (b), only the five oligarchs are integrated. Arrows in panel (a) mark the times when 15%, 50%, and 85% of  $N_{\text{real}} = 200$  realizations (integrations) experience the first ejection of an oligarch. Vertical lines separate various phases of evolution discussed in §2.2.3.

### 2.2.3. Results: Eccentricity and Inclination Growth (“Stirring Curves”)

Fig. 1 tracks the median eccentricity,  $e_{50}(t)$ , of all oligarchs. The sample from which the median is drawn always contains  $N_{\text{all}} = 1000$  objects, regardless of whether oligarchs collide or are ejected. When computing the median, we adopt the following rules: ejected oligarchs have their eccentricities set equal to 1 (but remain part of the sample); an oligarch that collides with either the Sun, Jupiter, or Saturn has its eccentricity set equal to 1; and oligarchs that collide with other oligarchs are still counted as separate objects and are each assigned an eccentricity equal to the current eccentricity of the merged body. Experiments with alternative sets of rules produced no qualitative changes to our results.

The resultant “stirring curves” of Fig. 1 exhibit a variety of behaviors. We first discuss the case when Jupiter and Saturn are omitted from the integrations (Fig. 1b). As annotated in Fig. 1b, we distinguish four phases of viscous stirring:

1. *Distant Conjunctions:* At early times  $t \lesssim 500$  yr, planetary orbits do not cross and  $e_{50}$  grows roughly linearly with time. A linear dependence is expected from viscous stirring by distant conjunctions, i.e., conjunctions between oligarchs that are not nearest neighbors. To derive the  $t^1$  scaling, we estimate using the impulse approximation that a conjunction between two oligarchs separated by distance  $x < a$  imparts eccentricities on the order of

$$\Delta e \sim \mu \left( \frac{a}{x} \right)^2 \quad (2)$$

to both bodies, provided they have eccentricities less than  $\Delta e$  prior to conjunction. For a given oligarch, a total of  $N \sim \Sigma a x / m$  oligarchs all reside about the same distance  $x$  away, where  $\Sigma$  is

the mass surface density of oligarchs. Conjunctions with these oligarchs occur over the synodic period

$$t_{\text{syn}} \sim \frac{a}{x} t_{\text{orb}}, \quad (3)$$

where  $t_{\text{orb}}$  is the orbital period. Then

$$\frac{de}{dt} \sim N \frac{\Delta e}{t_{\text{syn}}} \sim \frac{\Sigma a^2}{m_{\odot}} \frac{1}{t_{\text{orb}}} \sim \text{constant} \quad (4)$$

as roughly observed in Fig. 1. As time elapses, ever closer neighbors at smaller  $x$  drive the stirring. This reasoning matches that given by GLS04 in their treatment of viscous stirring in the shear-dominated regime; their eqn. (33) is identical in form to our eqn. (4). The  $t^1$  scaling is also derived by Collins & Sari (2006) and Collins, Schlichting, & Sari (2007). These latter studies concentrate on the limit  $N_{\text{olig}} \gg 1$ .

2. *Conjunctions with Nearest Neighbors:* At intermediate times  $500 \lesssim t(\text{yr}) \lesssim 1.5 \times 10^4$ , planetary orbits remain non-crossing but the eccentricity distribution hardly changes. Since the synodic period between nearest neighboring oligarchs is  $t_{\text{syn}} \sim 500$  yr, a given oligarch during this phase experiences repeated conjunctions with its nearest neighbor. Such repeated close encounters might be expected to produce chaotic motion and to cause eccentricities to random walk, in which case  $e_{50} \propto t^{1/2}$ . That this scaling is not observed implies that our 5 oligarchs do not behave in a strongly chaotic manner despite their close spacing. Indeed, we observe in our simulations that the epicyclic phases (true anomalies) of a given oligarch at successive conjunctions with its nearest neighbor do not vary completely randomly. Perturbations from conjunctions with a nearest neighbor apparently tend to cancel out during this second phase.

3. *Onset of Orbit Crossing:* The cancellations characterizing the preceding phase are not perfect, however. Eventually, from  $t \sim 1.5 \times 10^4$  yr to  $t \sim 5 \times 10^4$  yr, eccentricities surge as oligarchs start crossing orbits. The median eccentricity  $e_{50}$  surpasses the orbit-crossing value,  $e \approx 0.06$ , during this third phase.

Our finding that orbits cross in a few  $\times 10^4$  yr is consistent with numerical experiments by Chambers, Wetherill, & Boss (1996), who measure times required for close encounters to occur in initially circular, co-planar, multi-planet systems as a function of planet mass and orbital spacing. For reference, our spacing of  $5R_H$  corresponds to 4 “mutual Hill sphere radii” as defined by those authors.

4. *Orbit Crossing:* At late times  $t \gtrsim 5 \times 10^4$  yr, oligarchs routinely cross orbits and we observe  $e_{50} \propto t^{0.25}$ . We can reproduce this scaling using the following particle-in-a-box argument. An oligarch's random velocity  $v$  at time  $t$  is determined largely by its closest encounter with another oligarch up until that time. We call the impact parameter characterizing this closest encounter  $b_{\min}$ . From kinetic theory,  $nb_{\min}^2 vt \sim 1$ , where  $n \sim \Sigma \Omega / mv$  is the

number density of oligarchs and we have assumed that the random velocity distribution of oligarchs is isotropic. It follows that  $b_{\min} \propto 1/t^{1/2}$  and  $v \sim (Gm/b_{\min}^2)^{1/2} \propto t^{1/4}$ . This scaling agrees with that of eqn. (49) of GLS04 and that of eqn. (14) of C06.

When we restore Jupiter and Saturn to the integrations (Fig. 1a), we can still discern the four phases enumerated above. However, compared to the case without giants, some phase boundaries are shifted to earlier times, and  $e_{50}$  rises more quickly during some phases. Phase 1 transitions to phase 2a at  $t \approx 30$  yr; at this time, all oligarchs have undergone their first conjunctions with Jupiter and Saturn. Phase 2a transitions to phase 2b at  $t \approx 500$  yr; as in the case without giants, this transition marks the time when every oligarch has experienced about one conjunction with its nearest neighboring oligarch. During phase 2b, we witness the same remarkable near-constancy of  $e_{50} \approx 0.01$ . Finally, during phase 4 at  $t \gtrsim 3 \times 10^4$  yr, when oligarchs are on crossing orbits,  $e_{50} \propto t^{0.38}$ . Such growth outpaces that observed in the absence of the gas giants.

What about oligarch inclinations? In simulations without gas giants, we observe that the median inclination  $i_{50}$  remains fairly constant at the initial value of  $10^{-4}$  until phase 3. As orbits cross,  $\sin i_{50}$  surges up to  $\sim 0.05$ , and thereafter grows as  $t^{0.25}$  during phase 4, just as  $e_{50}$  does. By  $t = 10^7$  yr,  $i_{50} \approx 10^\circ$ . When Jupiter and Saturn are included,  $\sin i_{50} \propto t^{0.28}$  during phase 4. By  $t = 10^7$  yr,  $i_{50} \approx 10^\circ$ , as was the case without the gas giants. The modest growth of oligarchs' inclinations will limit the degree to which inclinations of KBOs are stirred (§3.3.2).

Not all of the different phases of viscous stirring that we observe are anticipated from the study of GLS04, which documents only the  $t^1$  scaling characterizing shear-dominated oligarchy (phase 1) and the  $t^{1/4}$  scaling characterizing the super-Hill, orbit-crossing regime (phase 4, no giants). Their analysis misses the intermediate phase 2 of slow-to-no growth just prior to orbit crossing, and the significant roles that Jupiter and Saturn play in accelerating viscous stirring during phase 4 ( $t^{0.38}$  vs.  $t^{1/4}$ ). That differences exist is not too surprising, as their analysis is rooted in the large  $N_{\text{olig}} \gg 1$  limit, whereas for our system,  $N_{\text{olig}} = 5$ . More importantly, we take nearest-neighboring oligarchs to be separated by 5 Hill sphere radii, as dictated by the extent of an oligarch's feeding zone in a shear-dominated disk (Greenberg et al. 1991), whereas the order-of-magnitude equations of GLS04 governing shear-dominated oligarchy assume the separation is closer to  $\sim 1$  Hill sphere radius. In this regard, we present in Figure 2 viscous stirring curves for cases where the oligarch separation is  $3R_H$  and  $7R_H$  (corresponding to coefficients in eqn. (1) of 1.5 and 3.5, respectively). Without gas giants, for a separation of  $3R_H$ , phases 2 and 3 disappear, leaving only phases 1 and 4 as originally envisioned by GLS04. The time to orbit crossing varies from  $\sim 300$  yr to  $\sim 2 \times 10^6$  yr as the spacing changes from 3 to 7 Hill radii. This extreme sensitivity to spacing was also found by Chambers et al. (1996). Including gas giants, however, reduces this sensitivity, as Fig. 2a shows.

The actual oligarchic spacing might only be determined by careful numerical simulations of accretion and orbital

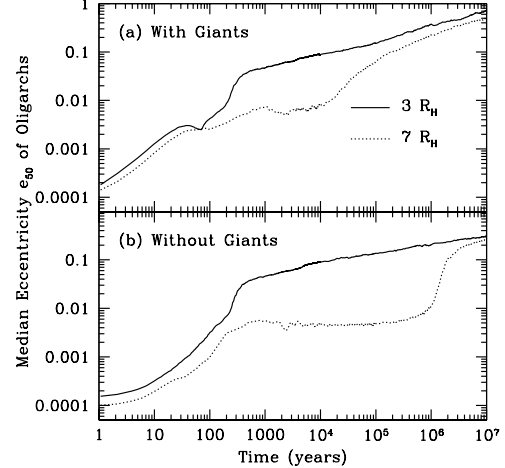


FIG. 2.— Viscous stirring of oligarchs, in the absence of dynamical friction, for assumed oligarchic spacings of  $3R_H$  and  $7R_H$ . Data are generated and presented in the same way as for Fig. 1, but only median eccentricities are displayed. Without the gas giants, the same 4 phases characterizing viscous stirring for  $5R_H$  (Fig. 1) are evident for  $7R_H$ . A spacing of  $3R_H$  produces systems sufficiently chaotic that phase 2b is indiscernible. Adding the gas giants, however, reduces the sensitivity of the results to the oligarchic spacing.

migration. We adopt in this paper a standard value of  $5R_H$ , identical to that assumed by GLS04, and motivated by studies of shear-dominated accretion by Greenberg et al. (1991). Shorter spacings seem less attractive insofar as they will produce smaller isolation masses for a given disk surface density.

The intermediate phase of slow-to-no growth of eccentricity that characterizes oligarchic spacings  $\geq 5R_H$  will prove important in determining the threshold disk surface density below which dynamical friction cooling cannot balance viscous heating, i.e., the threshold surface density for the velocity instability (§3.2).

### 2.3. Dynamical Friction

Oligarchs grow from a disk of planetesimals. Those planetesimals that are not accreted exert dynamical friction on oligarchs. The conditions for velocity instability, and the ease with which survivors of the instability return to low-eccentricity, low-inclination orbits, depend on the strength of dynamical friction. We describe how we implement dynamical friction in our simulations in §2.3.1, present a test case in §2.3.2, and show that our implementation is compatible with the formulae of GLS04 in §2.3.3.

#### 2.3.1. Prescription

Consider a planet having an eccentricity and an inclination much greater than those of disk planetesimals. Dynamical friction reduces the planet's random (peculiar) velocity: the difference  $\vec{v} \equiv v\hat{v}$  between the orbital velocity of the planet and that of the mean disk flow. From Binney & Tremaine (1987, their eqn. 7-17),

$$\frac{d\vec{v}}{dt} = -\frac{2\pi G^2 m \rho}{v^2} \ln(1 + \Lambda^2) \hat{v}, \quad (5)$$

where  $\rho$  is the local mass density of the disk,  $m$  is the mass of the planet,  $G$  is the gravitational constant, and

$$\Lambda = \frac{b_{\max}(v^2 + 2\langle \sin^2 i_{\text{disk}} \rangle v_{\text{circ}}^2)}{Gm} \quad (6)$$

is the Coulomb parameter appropriate for dynamical friction in a Keplerian disk (Stewart & Ida 2000). For  $b_{\max}$ , the maximum impact parameter between the planet and a disk planetesimal, we adapt the expression of Stewart & Ida (2000; see the discussion following their eqn. 2-17):

$$b_{\max} = R_H + r (\langle \sin^2 i_{\text{disk}} \rangle + \sin^2 i)^{1/2}, \quad (7)$$

where  $r$  is the instantaneous distance between the planet and the system barycenter,  $R_H = (\mu/3)^{1/3}r$  is the Hill sphere radius, and  $\langle \sin^2 i_{\text{disk}} \rangle^{1/2} \ll 1$  is the inclination dispersion of disk planetesimals, held constant for each simulation (more on its precise value later). The term  $2\langle \sin^2 i_{\text{disk}} \rangle v_{\text{circ}}^2$  in eqn. (6) approximates the square of the velocity dispersion of disk planetesimals, where  $v_{\text{circ}}$  is the local mean disk speed. We take  $v_{\text{circ}}$  to equal the speed that the planet would have on a circular orbit about the Sun.

Usually it is assumed in writing eqn. (5) that  $\Lambda \gg 1$ . We do not make this assumption. In fact, we use eqns. (5)–(7) regardless of the magnitude of  $\Lambda$ . When  $\Lambda \ll 1$ , dynamical friction is in the shear-dominated regime. In §2.3.3, we justify our universal application of (5)–(7) by showing that these equations correctly reduce to forms appropriate to the shear-dominated case when  $\Lambda \ll 1$ .

We implement dynamical friction as follows. We are interested in the case where the oligarchs are so dynamically excited that each plunges through a vertically thin, dynamically cold disk of planetesimals twice per orbit. Specifically, we assume that the time a planet spends immersed in the disk,  $\Delta t \approx h/|v_z|$ , where  $h$  is the full vertical thickness of the disk and  $|v_z|$  is the vertical component of  $\vec{v}$  at the moment of disk crossing, is short compared to the orbital period,  $t_{\text{orb}} = 2\pi/\Omega$ . Equivalently,  $\sin i \gg \langle \sin^2 i_{\text{disk}} \rangle^{1/2}$ . At every disk crossing, a planet receives a specific impulse of

$$\begin{aligned} \Delta \vec{v} &\approx \frac{d\vec{v}}{dt} \Delta t \approx -\frac{2\pi G^2 m}{v^2} \ln(1 + \Lambda^2) \rho \Delta t \hat{v} \\ &\approx -\frac{2\pi G^2 m}{v^2} \ln(1 + \Lambda^2) \frac{\sigma}{|v_z|} \hat{v}, \end{aligned} \quad (8)$$

where  $\sigma$  is the disk surface density (height-integrated  $\rho$ ). At every timestep of the integration, we check whether the planet crosses through the disk, which is fixed to lie in the x-y plane. At moments of disk crossing, we apply a kick according to eqn. (8): we increment the velocity of the planet by  $\Delta \vec{v}$  but do not change the planet's position. We compute the difference velocity  $\vec{v}$  by subtracting the barycentric velocity of the planet from  $v_{\text{circ}} \hat{\phi}$ , where  $\hat{\phi}$  is the unit vector in the azimuthal direction. The kick is applied in the subroutine MDT\_HY.FOR in the MERCURY6 code, after the positions are advanced but before the velocities are updated for the second time by the interaction Hamiltonian.

For all our simulations, we fix  $\langle \sin^2 i_{\text{disk}} \rangle^{1/2} = 10^{-3}$ , a value sufficiently small that  $\sin i \gg \langle \sin^2 i_{\text{disk}} \rangle^{1/2}$  for all but a tiny fraction of the time. In other words, the

strength of dynamical friction in our simulations depends much more strongly on the planet's random speed  $v$  than on the much smaller random speeds of planetesimals (see eqns. 6–7). Planetesimals can maintain low velocity dispersions by inelastic collisions or by gas drag.

Our scheme for dynamical friction damps orbital inclinations relative to the x-y (disk) plane. The inclination may become so small that  $\Delta t \propto 1/\sin i$  exceeds  $t_{\text{orb}}$ , at which point the planet is immersed within the disk and our impulse approximation breaks down. To account for this possibility, we arbitrarily set  $\Delta t = \min(h/|v_z|, 0.025/\Omega)$ . Our softening prescription slows but does not stop the damping of inclination and eccentricity for  $\sin i \lesssim 0.004$ . The softening might represent slight misalignments between the planet's orbital plane and the disk midplane, which in reality will be warped. We have verified that our principal findings, described in §3, do not depend sensitively upon the details of this prescription. While the precise values of the inclinations that we compute are clearly not very meaningful, we expect that our results are still qualitatively correct, i.e., the code correctly identifies when mutual inclinations between planetary orbits are large ( $> 1$  rad) and small ( $\ll 1$  rad).

The main virtue of our prescription for dynamical friction is its simplicity. We need only specify the disk surface density  $\sigma(r)$ , not the volumetric density  $\rho(r, z)$ , and we need only apply dynamical friction at disk crossings. The main shortcoming of our prescription is that it does not account for the response of the disk to the planets. The clearing of gaps and the generation of time-dependent, non-axisymmetric structures (see, e.g., Goldreich & Tremaine 1982) will alter the gravitational back-reaction of the disk onto embedded planets in ways that could be significant but that we (and GLS04) do not capture. For ways to model the response of the planetesimal disk more realistically, see Lithwick & Chiang (2007) and Levison & Morbidelli (2007).

### 2.3.2. Test with Single Planet

We test our prescription for dynamical friction in the case of a single planet interacting with a disk. The disk has constant surface density  $\sigma = 1 \text{ g/cm}^2$ . A Neptune-mass oligarch is placed on an orbit having initial semi-major axis  $a_{\text{init}} = 20 \text{ AU}$  and initial eccentricity and inclination such that  $e_{\text{init}} = \sin i_{\text{init}} = 0.3$ . Two cases are considered, one where the initial argument of perihelion  $\omega_{\text{init}} = 0$  and another where  $\omega_{\text{init}} = \pi/2$ . The evolution of  $e(t)$  and  $i(t)$  depends on  $\omega_{\text{init}} \bmod \pi$ .

Fig. 3 displays the resultant evolution. The planet's eccentricity and inclination both drop precipitously toward zero after a time on the order of  $10^6 \text{ yr}$ ; the exact time varies by a factor of 3 between our choices for  $\omega_{\text{init}}$ . The semi-major axis can increase or decrease. It changes by 3–13%, on the order of but less than the starting eccentricity.

We check our numerical results by comparing them to the following approximate analytic solution. Since the kick  $\Delta \vec{v}$  is applied twice per orbit, we write

$$\frac{d\vec{v}}{dt} \approx -\frac{2\Delta\vec{v}}{t_{\text{orb}}}$$

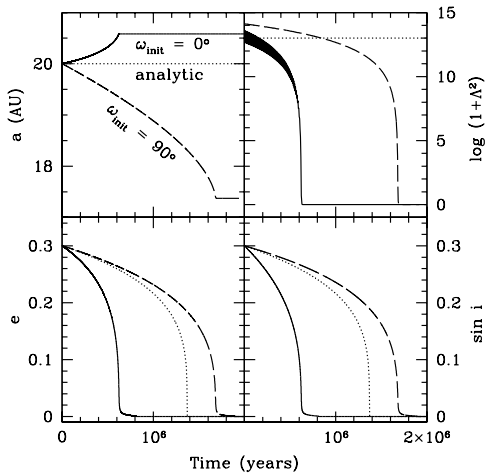


FIG. 3.— Test of our prescription for dynamical friction. We calculate the orbital evolution of a single Neptune-mass planet interacting with a disk of surface density  $\sigma = 1 \text{ g/cm}^2$ . Solid curves denote the evolution when the planet's initial argument of pericenter  $\omega_{\text{init}} = 0$  (so that the orbit intersects the disk at pericenter and apocenter), while dashed curves correspond to  $\omega_{\text{init}} = \pi/2$  (so that the orbit intersects the disk at quadrature). Dotted curves represent our analytic solution (11) which assumes a constant semi-major axis  $a$  and Coulomb parameter  $\Lambda$ .

$$\approx -4\pi \ln(1 + \Lambda^2) \frac{G^2 \sigma m}{t_{\text{orb}}} \frac{\vec{v}}{v^3 |v_z|}. \quad (9)$$

We set  $e = \sin i$  and make the following approximations:  $\vec{v} = (e\hat{p} + i\hat{z})\Omega a$ ,  $v = \sqrt{2}e\Omega a$ , and  $|v_z| = i\Omega a$ . Here  $\hat{p}$  and  $\hat{z}$  are unit vectors that lie parallel and perpendicular to the disk, respectively. Then (9) simplifies to

$$\frac{de}{dt} = -\frac{\ln(1 + \Lambda^2)}{\sqrt{2}} \frac{G\sigma}{\Omega a} \frac{m}{m_{\odot}} \frac{1}{e^3}, \quad (10)$$

with an analogous equation for  $i$ . For fixed  $\Lambda$  and  $a$ , eqn. (10) integrates to

$$e = \left( e_{\text{init}}^4 - \frac{4 \ln(1 + \Lambda^2)}{\sqrt{2}} \frac{m}{m_{\odot}} \frac{G\sigma}{\Omega a} t \right)^{1/4}. \quad (11)$$

The eccentricity (equivalently, inclination) vanishes in a finite time

$$t_{\text{vanish}} = \frac{\sqrt{2}}{4 \ln(1 + \Lambda^2)} \frac{m_{\odot}}{m} \frac{\Omega a}{G\sigma} e_{\text{init}}^4. \quad (12)$$

We overlay eqn. (11) in Fig. 3, taking as representative values  $a = a_{\text{init}} = 20 \text{ AU}$  and  $\ln(1 + \Lambda^2) = \ln(1 + \Lambda_{\text{init}}^2) = 13$ . The analytic solution lies between the two numerical solutions. We consider the agreement acceptable.

### 2.3.3. Connecting Our Prescription to GLS04

Our equations can be re-cast into the same forms as those of GLS04, under the assumption  $e = i$ . We start with eqn. (9) and substitute  $|v_z| = v/\sqrt{2}$ ,  $t_{\text{orb}} = 2\pi/\Omega$ , and  $m = (4\pi/3)\rho_p R_p^3$ , where  $\rho_p$  and  $R_p$  are the internal density and physical radius of the planet:

$$\frac{1}{v} \frac{dv}{dt} = -2^{3/2} \ln(1 + \Lambda^2) \sigma \Omega \frac{4\pi G^2 \rho_p R_p^3}{3v^4}. \quad (13)$$

We next recognize that  $4\pi G^2 \rho_p R_p^4 / 3 = 3v_{\text{esc},p}^4 / 16\pi$ , where  $v_{\text{esc},p}$  is the escape velocity from the surface of the planet. Then eqn. (13) simplifies to

$$\frac{1}{v} \frac{dv}{dt} = -\frac{3\sqrt{2}}{8\pi} \ln(1 + \Lambda^2) \frac{\sigma \Omega}{\rho_p R_p} \left( \frac{v_{\text{esc},p}}{v} \right)^4. \quad (14)$$

When  $\ln(1 + \Lambda^2)$  is a constant of order unity, eqn. (14) matches the form of eqn. (45) of GLS04, evaluated using the first line of their eqn. (46), with their planetesimal random velocity  $u$  replaced by  $v$  (since  $v > u$ ; see their section 5.5, end of first paragraph). This formula describes dynamical friction in the dispersion-dominated regime, where  $v$  exceeds the Hill velocity  $v_H = \Omega R_H$ .

On the other hand, it is possible for  $\Lambda \ll 1$ . This happens, according to (6)–(7), when  $v \sim \sqrt{2}i\Omega \ll \sqrt{Gm/R_H} \sim v_H$  (terms proportional to  $\langle \sin^2 i_{\text{disk}} \rangle^{1/2} = 10^{-3}$  are negligible). In this shear-dominated regime,

$$\Lambda \approx \frac{R_H v^2}{Gm} \ll 1, \quad (15)$$

$\ln(1 + \Lambda^2) \approx \Lambda^2$ , and eqn. (14) reduces to

$$\begin{aligned} \frac{1}{v} \frac{dv}{dt} &= -\frac{3}{\pi\sqrt{2}} \frac{\sigma \Omega}{\rho_p R_p} \left( \frac{R_H}{R_p} \right)^2 \\ &= -\frac{3}{\pi\sqrt{2}} \frac{\sigma \Omega}{\rho_p R_p} \frac{1}{\alpha^2}, \end{aligned} \quad (16)$$

where we have defined, following GLS04,  $\alpha \equiv R_p/R_H$ . Eqn. (16) matches, to within a numerical constant, eqn. (45) of GLS04, evaluated using the second line of their eqn. (46).

We conclude that our treatment of dynamical friction is compatible with that of GLS04.

## 3. RESULTS

We present the results of simulations that combine viscous stirring due to multiple oligarchs, with dynamical friction due to a planetesimal disk.

### 3.1. Initial Conditions and Integration Times

Each system begins with either  $N_{\text{olig}} = 5, 4$ , or  $3$  oligarchs, together with the gas giants, Jupiter and Saturn. Initial conditions are the same as those described in §2.2.1, except that initial eccentricities and inclinations of oligarchs are such that  $e_j = \sin i_j = 10^{-2}$ . Initial inclinations are therefore ten times larger than the assumed inclination dispersion of disk planetesimals ( $\langle \sin^2 i_{\text{disk}} \rangle^{1/2} = 10^{-3}$ ). Initial eccentricities are the same as those that characterize phase 2b of the viscous stirring curves (Fig. 1a). Planetary orbits initially do not cross.

Dynamical friction is exerted by a disk of constant surface density  $\sigma$  which extends from a barycentric radius of 12.5 AU to 45 AU. The outer boundary coincides with the location of the classical Kuiper belt (C06). The inner boundary is less well motivated. It is chosen so that the oligarchs reside initially inside the disk while the gas giants do not. We explore values for  $\sigma$  ranging from 0.4 to  $0.001 \text{ g/cm}^2$ . For reference, the initial surface density in oligarchs is  $\Sigma \approx 1.5 \text{ g/cm}^2$ .

In a subset of runs, we include 400 test particles representing large KBOs. These feel the gravity of the planets but do not feel dynamical friction from the disk (see §2.1). Initial semi-major axes of test particles range from  $a = 40$  to  $45$  AU, and initial eccentricities and inclinations are such that  $e = \sin i = 10^{-2}$ . For all planets and KBOs, initial longitudes of ascending node, longitudes of pericenter, and mean anomalies are randomly chosen from uniform distributions between 0 and  $2\pi$ .

Settings for the MERCURY6 code are the same as those given in §2.2.1, except for the duration of integration. The integration automatically halts when there are a catastrophic number of ejections, i.e., when the only massive bodies remaining include the Sun, Jupiter, Saturn, and one oligarch (which may have collided with other oligarchs). In the absence of such an event, each system is integrated first to  $t = 2 \times 10^7$  yr. If the planets seem to have stabilized at that time—i.e., their eccentricities no longer grow—then we stop the integration and record the outcome as final. Otherwise, we repeat this test as necessary at  $5 \times 10^7$  yr and  $1 \times 10^8$  yr.

By  $t = 1 \times 10^8$  yr, most but not all realizations stabilize. Excluding systems that are stopped abruptly once only three planets remain, we find that  $\lesssim 10\%$  of systems have undergone a close encounter (here defined to occur when the distance between any two planets is less than 1 Hill radius) within the last  $10^7$  yr of the integration, for  $N_{\text{olig}} = 5$  and all values of  $\sigma$  tested. For  $N_{\text{olig}} = 4$  and 3, the corresponding fractions are  $\lesssim 10\%$  and  $\lesssim 1\%$ . Those realizations that do not stabilize by  $t = 1 \times 10^8$  yr are typically characterized by small values of  $\sigma \lesssim 0.006 \text{ g/cm}^2$  (i.e., relatively weak dynamical friction) and one oligarch remaining on an eccentric orbit that extends well past the outer edge of the disk. For these low values of  $\sigma$ , the number of ejected oligarchs that we report will be underestimated, but not in a way that changes our qualitative conclusions.

The initial conditions just summarized apply to all results in the following two sections, §§3.2–3.3. An alternative set of initial conditions, motivated by the findings in those sections, and results pertaining thereto are presented in §3.4.

### 3.2. Threshold Disk Surface Densities for Instability

Oligarchs cross orbits when the disk surface density  $\sigma$  is so low that dynamical friction cooling cannot compete with viscous stirring. GLS04 estimate the critical surface density for instability to be on the order of the surface density of oligarchs:  $\sigma_{\text{crit}} \sim \Sigma$  (see also Chiang & Lithwick 2005 for a correction in the derivation of this result). How well does this criterion predict the onset of instability for our system of  $N_{\text{olig}} = 5$  oligarchs?

As noted in §2.2, the rates of eccentricity growth (viscous stirring) exhibited in our N-body integrations differ from those estimated by GLS04. Specifically, our rates are slower, as evidenced by the period of slow-to-no growth of eccentricity (phase 2b) in Fig. 1a. Overestimating the vigor of viscous stirring leads to overestimates for  $\sigma_{\text{crit}}$ . We try to predict  $\sigma_{\text{crit}}$  ourselves by drawing from the numerical results of §2.2. We observe in Fig. 1a that after a time  $t_{\text{unstable}} \sim 5 \times 10^3$  yr, eccentricities surge rapidly to crossing values.<sup>6</sup> Therefore

<sup>6</sup> Chambers et al. (1996) provide fitting formulae for  $t_{\text{unstable}}$

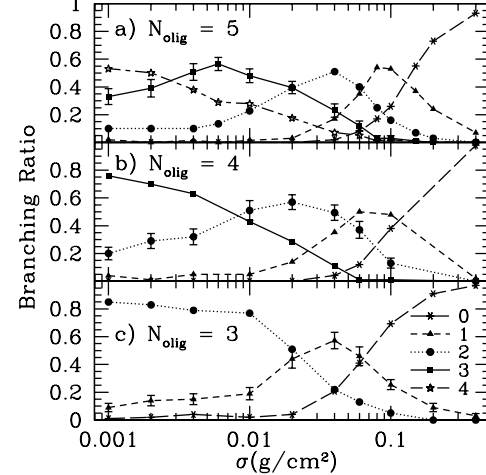


FIG. 4.—Branching ratios for the outcome of the velocity instability, for systems that include dynamical friction with a disk of surface density  $\sigma$ . For comparison, the initial surface density in oligarchs is  $\Sigma \approx 1.5 \text{ g/cm}^2$ . Systems begin with Jupiter, Saturn, and either  $N_{\text{olig}} = 5$  (top panel), 4 (middle panel), or 3 (bottom panel) oligarchs. Different symbols denote the fraction of realizations that result in 0, 1, 2, 3, or 4 ejections of oligarchs, whether collisionally merged or not. Few oligarchs collide in these simulations; the fraction of realizations that result in 1 collision is less than 20% for all values of  $\sigma$  tested, and the fraction of realizations that result in  $> 1$  collision is  $< 1\%$ . To produce  $\geq 1$  ejection with  $> 20\%$  probability requires  $\sigma \lesssim \Sigma/10$ . Standard error bars due to counting statistics are given for curves corresponding to  $N_{\text{olig}} - 2$  ejections.

for oligarchs to cross orbits, eccentricities must not be allowed to vanish by dynamical friction before  $t_{\text{unstable}}$ :

$$t_{\text{vanish}} > t_{\text{unstable}}. \quad (17)$$

Using (12) for  $t_{\text{vanish}}$ , we find that (17) translates into  $\sigma < \sigma_{\text{crit}}$ , where

$$\sigma_{\text{crit}} \sim \frac{\sqrt{2}}{4 \ln(1 + \Lambda^2)} \frac{m_{\odot}}{m} \frac{\Omega a e_{\text{init}}^4}{G t_{\text{unstable}}} \quad (18)$$

$$\sim 0.2 \text{ g/cm}^2 \sim 0.1 \Sigma. \quad (19)$$

The numerical evaluation takes  $a = 19.4$  AU,  $e_{\text{init}} = 0.01$  (the value appropriate to phase 2b of the viscous stirring curves in Fig. 1a; the median eccentricity does not rise above 0.01 for  $t < t_{\text{unstable}}$ ), and  $\ln(1 + \Lambda^2) = \ln(1 + \Lambda_{\text{init}}^2) = 0.02$ .

Our semi-empirical estimate for  $\sigma_{\text{crit}}$  finds support in Fig. 4a, which documents, for all runs starting with  $N_{\text{olig}} = 5$  oligarchs, the frequency of incidence of outcomes (“branching ratios”) as a function of  $\sigma$ . Instability and the subsequent ejection of 1 and only 1 oligarch is the dominant outcome for  $\sigma = 0.1 \text{ g/cm}^2 \approx 0.07\Sigma$ . For  $\sigma \gtrsim 0.3\Sigma$ , more than 90% of realizations produce no ejection. Fig. 5 displays a sample simulation for  $\sigma \approx 0.07\Sigma$  in which 1 oligarch escapes before the system stabilizes.

Figs. 4b and 4c supply branching ratios for  $N_{\text{olig}} = 4$  and 3. To produce the same number of ejections with smaller  $N_{\text{olig}}$  (less viscous stirring) requires smaller  $\sigma$  (less dynamical friction). For example, for  $N_{\text{olig}} = 3$ , the ejection of 1 and only 1 oligarch is the dominant

as functions of oligarch mass and orbital spacing, but only for the case without the gas giants Jupiter and Saturn.

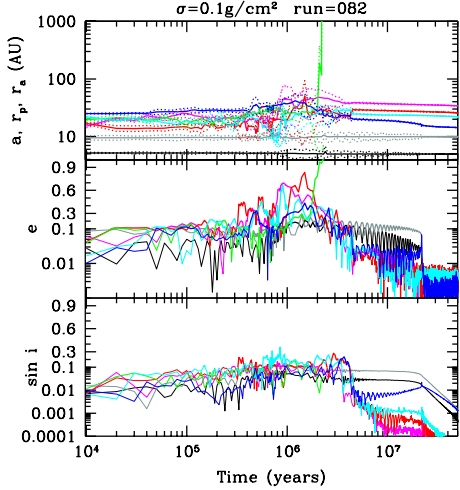


FIG. 5.— Typical realization for  $\sigma = 0.1 \text{ g/cm}^2 \approx 0.07\Sigma$  in which 1 oligarch escapes before the system stabilizes. The top panel plots semi-major axis (solid curves), and periastron and apastron distances (dotted curves) for each of the seven planets. Eccentricities (middle panel) and inclinations (bottom panel) are plotted using a mixed log-linear ordinate. Black curves refer to Jupiter, gray curves refer to Saturn, and remaining colored curves refer to the five oligarchs.

outcome for  $\sigma \approx 0.03\Sigma$ , occurring in about 60% of realizations. The corresponding  $\sigma$  for  $N_{\text{olig}} = 4$  is  $0.05\Sigma$ .

### 3.3. Runs with Two Surviving Oligarchs (Solar-System-Like Outcomes)

While  $\sigma_{\text{crit}} \sim 0.1\Sigma$  roughly characterizes the onset of instability and the subsequent ejection of a single oligarch, the disk surface density must be reduced below  $\sigma_{\text{crit}}$  to produce more than 1 ejection in a large fraction of runs. To generate an outcome reminiscent of our solar system starting with  $N_{\text{olig}} = 5$  requires 3 ejections and the survival of 2 oligarchs. According to Fig. 4a, such an outcome occurs with a maximum probability of  $\sim 50\%$  for  $\sigma \approx 0.01 \text{ g/cm}^2 \approx 0.007\Sigma$ . The probability exceeds 20% for all values of  $\sigma \lesssim 0.03\Sigma$  that we tested.

Figs. 4b and 4c indicate that for  $N_{\text{olig}} = 4$  and 3, the values of  $\sigma$  most likely to produce 4-planet systems (Jupiter, Saturn, plus 2 oligarchs) are  $\sim 0.01\Sigma$  and  $\sim 0.03\Sigma$ , respectively. The probabilities for generating 4-planet systems starting with  $N_{\text{olig}} = 4$  or 3 reach large maximum values of about 50%, and remain above 20% over a considerable range in  $\sigma$ , up to  $\sim 0.07\Sigma$  in the case  $N_{\text{olig}} = 3$ .

The vast majority of the resultant 4-planet systems are correctly ordered; they contain, in order of increasing semi-major axis, Jupiter, Saturn, and 2 oligarchs. Moreover, in most of these systems, the surviving planets have not experienced a collision. In the following sub-sections we further quantify the properties of these correctly ordered, collisionally unmodified, 4-planet systems, comparing them to those of the solar system. We refer to the 2 surviving oligarchs in each of these systems as Uranus and Neptune.

#### 3.3.1. Final Semi-Major Axis Distributions

Because packed oligarchies evolve chaotically, we can only meaningfully compute probability distributions for their final semi-major axes. Fig. 6 illustrates how these distributions depend on  $\sigma$ , for realizations starting with

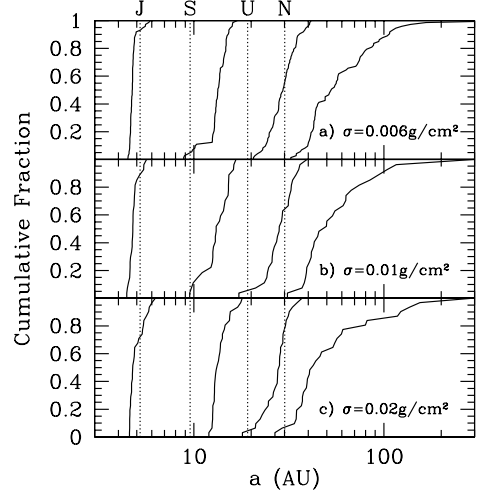


FIG. 6.— Cumulative distributions of final semi-major axes of systems that contain, in order of increasing semi-major axis, Jupiter, Saturn, and two oligarchs (Uranus and Neptune), each with their original mass. These 4-planet systems result from integrations originally containing 7 planets ( $N_{\text{olig}} = 5$ ). Each panel corresponds to simulations performed with the disk surface density  $\sigma$  indicated. Vertical lines mark the current semi-major axes of the giant planets in our solar system. Apart from a tendency for Saturn and Neptune to be pulled toward the inner ( $a = 12.5 \text{ AU}$ ) and outer ( $a = 45 \text{ AU}$ ) edges of the disk with increasing  $\sigma$  (increasing dynamical friction), the characteristic final semi-major axes do not depend on  $\sigma$ . Saturn, Uranus, and Neptune have final orbits too large compared to their actual counterparts in the solar system.

$N_{\text{olig}} = 5$ . Increasing  $\sigma$  increases dynamical friction and therefore tends to pull Saturn and Neptune, whose orbits lie near disk boundaries, into the disk. For example, if Saturn's orbital apocenter intersects the disk while its pericenter remains outside the disk, then dynamical friction will circularize the orbit by raising the pericenter closer to apocenter. The kinks in the distribution functions for Saturn in Figs. 6a and 6b are located at  $a = 12.5 \text{ AU}$ , exactly at the inner disk edge. The kink vanishes in Fig. 6c. For the simulations in Fig. 6c, dynamical friction is strong enough to pull Saturn's orbit wholly into the disk at  $a \geq 12.5 \text{ AU}$ .

To improve statistics, we ignore these small artifacts of our disk boundary conditions and pool together  $N_{\text{real}} = 438$  realizations, all of which start with  $N_{\text{olig}} = 5$  and produce 4-planet systems, but have a variety of  $\sigma$ 's between 0.001 and  $0.1 \text{ g/cm}^2$ . From this pool we construct the distribution of final semi-major axes shown in Fig. 7a. Clearly, most realizations end with Saturn, Uranus, and Neptune on orbits too large compared to their actual counterparts in the solar system. Furthermore, Jupiter typically migrates inward as a consequence of ejecting several oligarchs outward. The excessively large orbits of Saturn, Uranus, and Neptune are a consequence of those planets having scattered oligarchs inward to Jupiter.

Though they only comprise (given our assumed initial conditions) a few percent of outcomes for  $\sigma = 0.02 \text{ g/cm}^2$ , some realizations better resemble the solar system insofar as Uranus and Neptune have final semi-major axes less than 30 AU. Fig. 8 showcases an example. Even for this simulation, however, Saturn's final orbit is 3 AU larger than its actual one.

Reducing the number of starting oligarchs significantly lessens the problem of excessive migration. Figs. 7b and 7c show final semi-major axis distributions corresponding

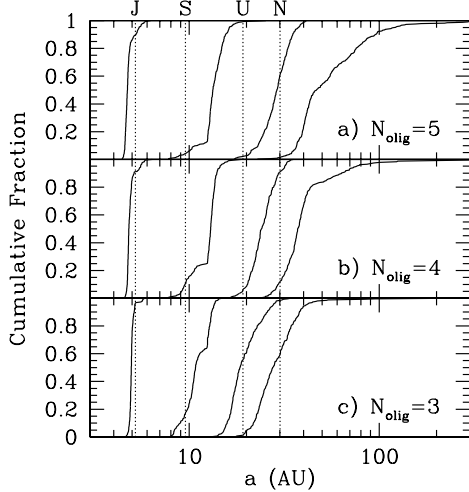


FIG. 7.— Cumulative distributions of final semi-major axes of correctly ordered, collision-free, 4-planet systems, shown for different starting values of  $N_{\text{olig}}$ . Each panel combines integrations performed with a variety of  $\sigma$ 's between 0.001 and  $0.1 \text{ g/cm}^2$ . Kinks in the distributions for Saturn and Neptune are artifacts of our assumed disk boundaries at  $a = 12.5 \text{ AU}$  and  $45 \text{ AU}$ . Vertical lines mark the current semi-major axes of solar system giants. Decreasing  $N_{\text{olig}}$  shrinks the final orbits for Saturn, Uranus, and Neptune. Final orbits resembling those of the current solar system are most easily produced for  $N_{\text{olig}} = 3$ .

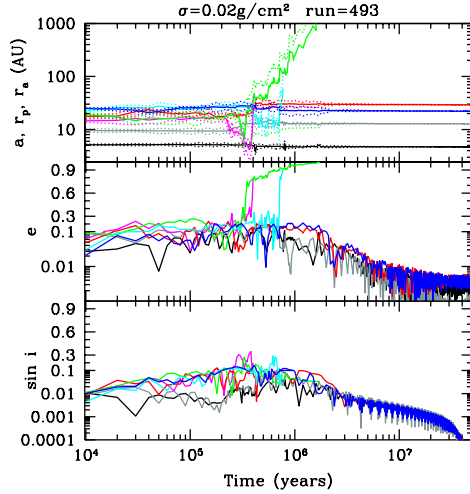


FIG. 8.— Example realization for  $\sigma = 0.02 \text{ g/cm}^2$  and  $N_{\text{olig}} = 5$  in which 3 oligarchs (denoted by magenta, green, and cyan curves) escape before the system stabilizes. The remaining 2 oligarchs (blue and red) have final, nearly circular and co-planar orbits inside 30 AU, similar to those of Uranus and Neptune. Such an outcome occurs with a frequency of a few percent for  $\sigma = 0.02 \text{ g/cm}^2$ .

to  $N_{\text{olig}} = 4$  and 3, respectively. Outcomes for  $N_{\text{olig}} = 3$  are most solar-system-like. In §3.4 we will experiment with initial conditions to demonstrate that a level of agreement comparable to that displayed in Fig. 7c for  $N_{\text{olig}} = 3$  can also be obtained for  $N_{\text{olig}} = 4$ .

### 3.3.2. Stirring of KBOs

Fig. 9 describes how the test particles (KBOs), initially distributed in a dynamically cold ring at  $a = 40$ – $45 \text{ AU}$ , are stirred by oligarchs, for the same  $N_{\text{olig}} = 5$  simulation (Fig. 8) which places Uranus and Neptune on final orbits inside 30 AU. Simulation data are collected at  $t = 5 \times 10^7 \text{ yr}$ . For comparison, Fig. 9 also plots data

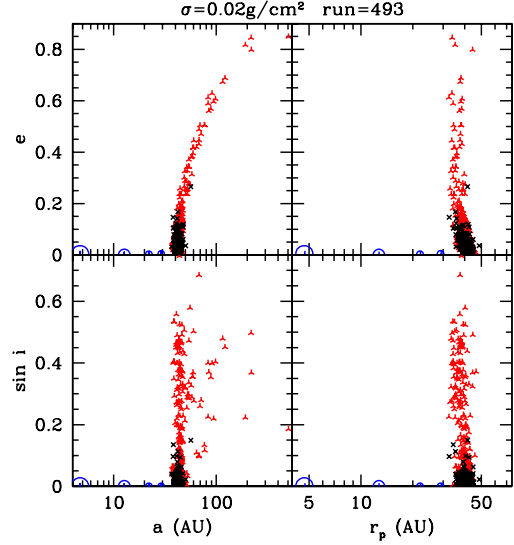


FIG. 9.— Orbital elements of simulated KBOs (black crosses) at  $t = 5 \times 10^7 \text{ yr}$ , for the same simulation shown in Fig. 8. Eccentricities and inclinations are displayed against either semi-major axis  $a$  or perihelion distance  $r_p$ . For comparison we show orbital elements of known classical and scattered (non-resonant) KBOs (red inverted Y's) from C06. Orbital elements of surviving planets (Jupiter, Saturn, and the two oligarchs) are shown as blue circles. Simulated KBOs for this run do not exhibit the large eccentricities and inclinations characterizing actual KBOs, but see Figs. 11 and 14 for other examples.

for actual KBOs that do not reside in any strong mean-motion resonance. These objects, taken from C06, comprise both low- $e$  classical and high- $e$  scattered KBOs as classified by the Deep Ecliptic Survey (Elliot et al. 2005). The simulated test particles have their eccentricities and inclinations excited up to  $\sim 0.1$ , values that match actual classical KBOs. But the simulated particles fail to embody the extreme degree of dynamical heating exhibited by scattered KBOs. Marauding oligarchs in this simulation stir planetesimals at 40–45 AU too briefly.

Since simulations with  $N_{\text{olig}} = 3$  more efficiently generate solar-system-like planetary spacings than do simulations with  $N_{\text{olig}} = 5$ , we can more thoroughly map out the possible extents to which KBOs are stirred for  $N_{\text{olig}} = 3$ . Figs. 10 and 11 document one simulation, representative of several percent of the solar-system-like realizations generated using  $N_{\text{olig}} = 3$ , in which KBOs are stirred considerably. Even here, however, the proportion of simulated KBOs that simultaneously attain inclinations  $i \gtrsim 10^\circ$  and perihelion distances  $r_p \gtrsim 35 \text{ AU}$  is less than observed. The proportion of simulated KBOs having eccentricities  $e \gtrsim 0.3$  also seems underrepresented.

### 3.4. More Compact Initial Conditions

As described in §§3.2–3.3, the simulations that begin with  $N_{\text{olig}} = 4$  or 5 oligarchs often do yield 4-planet systems, but the orbital spacings of the resultant systems do not match those of the solar system. Multiple ejections displace Jupiter too far inward and displace Saturn, Uranus, and Neptune too far outward. The problem of excessive spreading is exacerbated by the need to have Neptune conclude its orbital evolution by migrating smoothly and slowly outward from  $a \approx 23$  to 30 AU to produce the population of resonant KBOs (Murray-Clay

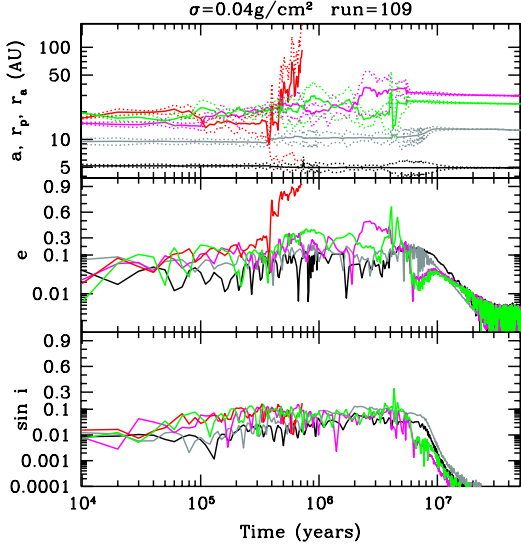


FIG. 10.— Example realization for  $N_{\text{olig}} = 3$  and  $\sigma = 0.04 \text{ g/cm}^2$  in which surviving planets have final orbits resembling those of the solar system (for an even closer match, see Fig. 13, generated using a revised set of initial conditions). Moreover, the KBOs in this simulation, shown in Fig. 11, are stirred considerably by oligarchs. Such an outcome represents several percent of runs generated using  $N_{\text{olig}} = 3$ .

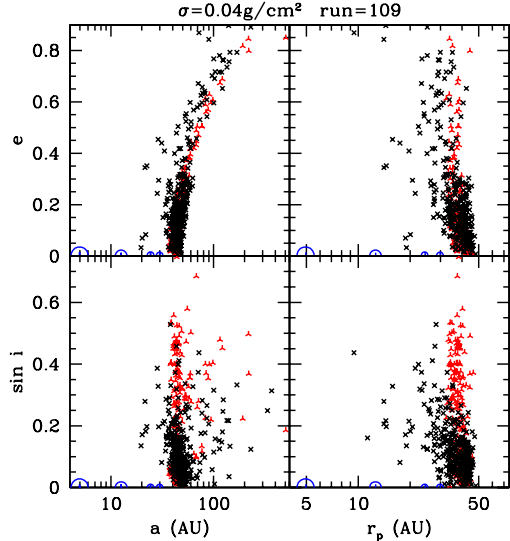


FIG. 11.— Orbital elements of simulated KBOs at  $t = 5 \times 10^7 \text{ yr}$ , for the same simulation shown in Fig. 10. In every panel except the one at the bottom left, simulated KBOs (black crosses) located to the left of observed KBOs (red inverted Y's) are unstable over the age of the solar system because of perturbations by the giant planets. Stable simulated KBOs (lying on top of and to the right of observed KBOs) exhibit large eccentricities and inclinations as a consequence of scattering by velocity-unstable oligarchs. Nevertheless, the simulations fail to reproduce the most extreme of observed scattered KBOs having  $\sin i \gtrsim 0.2$ .

& Chiang 2006, and references therein; but see Levison et al. 2006 for an alternative theory for the origin of resonant KBOs). This last constraint implies that our simulations should place Neptune on a final orbit near  $a \approx 23 \text{ AU}$ .

In this sub-section we attempt to remedy the problem of excessive spreading by adjusting our initial conditions. In anticipation of Jupiter's inward displacement, we locate that planet initially at  $a_J = 5.7 \text{ AU}$ . In anticipation

of Saturn's outward displacement, we set  $a_S = 8 \text{ AU}$  initially. The innermost oligarch is also shifted inwards, to  $a_1 = 12 \text{ AU}$ . Initial semi-major axes for remaining oligarchs are still given by eqn. (1):  $a_2$  through  $a_5$  equal 13.7, 15.5, 17.7, and 20.1 AU. Finally, so that all oligarchs lie initially inside the disk, we extend the inner edge of the disk inward to 10 AU. All remaining parameters remain unchanged from their values in §3.1.

The distribution of final semi-major axes for resultant 4-planet systems is given by Fig. 12, constructed in similar fashion to Fig. 7. The more compact initial configuration produces reasonably close matches to current orbital spacings in the solar system for  $N_{\text{olig}} = 4$ . Results for  $N_{\text{olig}} = 3$  are also acceptable if we allow for the subsequent outward migration of Neptune that is seemingly demanded by resonant KBOs (see first paragraph of this sub-section). The case  $N_{\text{olig}} = 5$  still suffers, however, from excessive spreading.

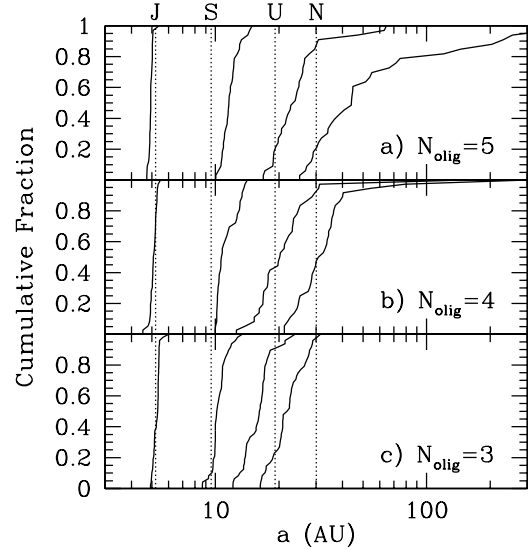


FIG. 12.— Same as Fig. 7, but generated using the more compact initial configuration described in §3.4. Runs starting with  $N_{\text{olig}} = 5$  oligarchs still produce final orbits for the 2 surviving oligarchs that are still too large compared to those of ice giants in our solar system. The case  $N_{\text{olig}} = 3$  produces ice giant orbits that are too small. Nevertheless,  $N_{\text{olig}} = 3$  is acceptable if we allow for subsequent outward migration of the ice giants. Such outward migration seems necessary to explain the origin of resonant KBOs (C06; but see Levison et al. 2006 for an alternative theory). Results for  $N_{\text{olig}} = 4$  are intermediate and produce orbital spacings most closely resembling those of the current solar system. Data for  $N_{\text{olig}} = 5, 4$ , and 3 are generated with runs having  $\sigma = 0.01, 0.04$ , and  $0.1 \text{ g/cm}^2$ , respectively.

Figs. 13 and 14 sample one simulation using the revised compact configuration for  $N_{\text{olig}} = 4$ . We highlight this simulation because it reproduces solar system properties, insofar as (1) Uranus and Neptune have final semi-major axes less than 30 AU, and (2) the Kuiper belt at 40–45 AU is significantly stirred. Though outcome (1) is not infrequent—occurring in, e.g., 16 out of 100 runs with  $\sigma = 0.04 \text{ g/cm}^2$  and  $N_{\text{olig}} = 4$ —outcome (2) is less probable, characterizing only several percent of runs already culled to satisfy (1). Most runs that satisfy (1) stir KBOs to eccentricities and inclinations of just a few percent. By contrast, the simulation showcased in Fig. 14 excites large eccentricities and inclinations simi-

lar to those sported by actual KBOs. Nevertheless, the most extreme of scattered KBOs, having perihelion distances  $r_p \gtrsim 40$  AU and inclinations  $i > 20^\circ$ , are still under-represented. In short, our revised compact configuration stirs KBOs to about the same degree as our original configuration.

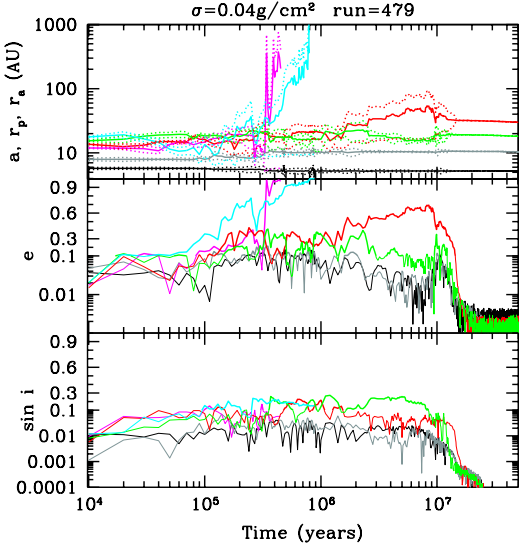


FIG. 13.— Similar to Fig. 10, except generated for  $N_{\text{olig}} = 4$  using the more compact initial configuration described in §3.4. The simulation starts with a total of 6 planets (Jupiter, Saturn, and 4 oligarchs) and ends with Jupiter, Saturn, and two oligarchs on orbits that closely match their actual counterparts in the solar system.

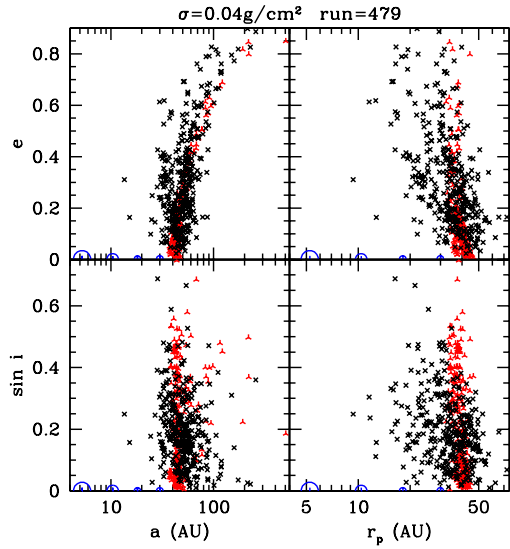


FIG. 14.— Orbital elements of simulated KBOs at  $t = 5 \times 10^7$  yr, for the same simulation shown in Fig. 13. The same remarks given in the caption to Fig. 11 concerning the stability of simulated KBOs apply here. Stable simulated KBOs, though stirred considerably by velocity-unstable oligarchs, fail to embody the large inclinations  $i \gtrsim 20^\circ$  exhibited by observed scattered KBOs.

#### 4. SUMMARY AND OUTLOOK

In §4.1, we answer the three questions posed in §1. In §4.2, we place our work in a broader context and mention some directions for future work.

#### 4.1. Answers to Questions Posed in §1

1. Of all our simulations that initially place  $N_{\text{olig}} = 5$  Neptune-mass planets between 15 and 25 AU, and that have disk surface densities  $\sigma \approx 0.1 \text{ g/cm}^2 \approx 0.07\Sigma$  (where  $\Sigma \sim 1.5 \text{ g/cm}^2$  is the original surface density in oligarchs), 50% result in the ejection of a single oligarch (Fig. 4). For runs that begin with  $N_{\text{olig}} = 4$  and 3 oligarchs, we achieve similar outcomes for  $\sigma/\Sigma \sim 0.05$  and  $\sim 0.03$ , respectively. Jupiter is responsible for the vast majority of ejections, which occur within  $\sim 10^7$  yr. The likelihood of a single ejection remains as high as 20% if the above  $\sigma$ 's are increased by factors of 2–3. Roughly speaking then, we find that instability and ejection require  $\sigma/\Sigma \lesssim 0.1$ . By comparison, GLS04 estimate that  $\sigma/\Sigma \lesssim 1$  for instability. The difference arises partly because nearest-neighboring oligarchs in our simulations are separated by 5 Hill sphere radii, whereas their analysis of shear-dominated oligarchy assumes the separation is closer to  $\sim 1$  Hill sphere radius. Our choice of  $5R_H$  is motivated by the half-width of an oligarch's annular feeding zone in a shear-dominated disk. This half-width spans  $2.5R_H$  (Greenberg et al. 1991). Because oligarchs separated by  $5R_H$  viscously stir each other more slowly (Fig. 1, phase 2) than do oligarchs separated by  $1R_H$ , we find a threshold value for  $\sigma$  lower than what GLS04 estimate.
2. For certain choices of  $\sigma$  and initial semi-major axes, systems starting with  $N_{\text{olig}} = 3$  or 4 oligarchs frequently end with 2 surviving oligarchs on nearly circular and co-planar orbits inside 30 AU (Figs. 7 and 12). For example, of all runs that (a) use our revised set of initial semi-major axes (§3.4), (b) begin with  $N_{\text{olig}} = 4$  oligarchs, and (c) have  $\sigma = 0.04 \text{ g/cm}^2 \approx 0.02\Sigma$ , 44% end with solar-system-like configurations in which the outermost surviving oligarch orbits inside 30 AU. This percentage decreases with increasing  $N_{\text{olig}}$ . This is because surviving oligarchs spread outward, well beyond the current orbit of Neptune, as they scatter more oligarchs inward for eventual ejection by Jupiter. To eject efficiently more than one oligarch requires that  $\sigma$  be reduced considerably below the previously mentioned threshold of  $\sim 0.1\Sigma$ . For example, we find that for  $N_{\text{olig}} = 4$  and our original set of initial semi-major axes (§2.2.1), setting  $\sigma \sim 0.02 \text{ g/cm}^2 \sim 0.01\Sigma$  maximizes the likelihood of 2 ejections at  $\sim 50\%$ .
3. In a small fraction of runs that successfully place Jupiter, Saturn, and 2 oligarchs on solar-system-like orbits inside 30 AU, test particles (KBOs) located initially in a dynamically cold ring at 40–45 AU have their eccentricities and inclinations considerably excited by velocity-unstable oligarchs. We observe maximum eccentricities of  $\sim 0.8$  and maximum inclinations of  $\sim 20^\circ$  (Figs. 11 and 14). In runs characterized by the greatest degrees of excitation, orbits of simulated KBOs resemble those of observed classical KBOs and some observed scattered KBOs. However, no run reproduces the large proportion of observed scattered KBOs having in-

clinations  $\gtrsim 20^\circ$ . There may also be a problem in generating enough KBOs having eccentricities  $\gtrsim 0.3$ , given the observational selection bias against finding such objects.

These results are complementary to those of Levison & Morbidelli (2007), who concentrate on the limit  $\sigma \gg \Sigma$  and find that they cannot produce solar-system-like outcomes. In comparison, we study the case  $\sigma \lesssim \Sigma$  and find positive results.

#### 4.2. Commentary

##### 4.2.1. The Compactness of Our Preferred Initial Conditions

We find that a shear-dominated oligarchy can readily produce a solar-system-like outcome if it contains just a few excess oligarchs—about 1 or 2 extra—and if the oligarchs initially reside inside 20 AU. We are driven to these parameters because to scatter excess oligarchs inward (toward Jupiter for eventual ejection), surviving oligarchs must be scattered outward. The right amount of outward spreading is achieved for suitably compact initial configurations and not too many ejections.

Our favored initial conditions are about as compact as those of Tsiganis et al. (2005), who place their outermost ice giant initially at 17 AU. By comparison, in our revised set of initial conditions for  $N_{\text{olig}} = 4$ , the outermost oligarch is located at 17.7 AU. But we stress that our study differs from theirs in that we base our initial conditions on considerations of shear-dominated oligarchic accretion. An ice giant cannot form at 17 AU within the gas photoevaporation time of a few  $\times 10^7$  yr without strong gravitational focussing (§1; Levison & Stewart 2001; GLS04). This need for gravitational focussing can be met by a highly dissipative disk of planetesimals (GLS04; Rafikov 2004). It is this disk, and the multiple ( $> 2$ ) ice giants that it spawns, that we have modeled.

Why such a disk would not form Neptune-mass oligarchs outside 20 AU is an open question. For some ideas on what limits the sizes of planetary systems, see Youdin & Shu (2002) and Youdin & Chiang (2004).

##### 4.2.2. Reducing the Disk Surface Density (“Clean-Up” and Migration)

Velocity instability and the ejection of a single oligarch require  $\sigma/\Sigma \lesssim 0.1$ . Ejecting more than 1 oligarch requires still lower values of  $\sigma/\Sigma \sim 0.01$ . How can  $\sigma$  reach such low values? Accretion and/or ejection of planetesimals by oligarchs are natural possibilities. The rate at which  $\sigma$  decreases, compared to the rate at which oligarchs stir each other, determines whether more than 1 oligarch escapes. If the rate of depletion of  $\sigma$  is sufficiently slow, then after the first oligarch escapes, surviving planets may occupy orbits so spread apart that they remain stable even as  $\sigma$  decreases further. On the other hand, if the rate of depletion is fast, then conditions required to eject more than 1 oligarch can be met. We leave investigation of the time dependence of  $\sigma$  for future work.

Given an initial surface density in oligarchs of  $\Sigma \sim 1 \text{ g/cm}^2$ , the disk surface densities relevant for instability and ejection range from  $\sigma \approx 0.1$  to  $0.01 \text{ g/cm}^2$ . These  $\sigma$ 's are still higher than surface densities characterizing the

Kuiper belt today, which are on the order of  $0.001 \text{ g/cm}^2$  (integrated over all KBO sizes). “Cleaning up” the disk mass remains an unsolved problem (GLS04). Again, the mass could either be accreted or ejected by surviving planets. Planetesimal ejection drives planetary migration. For Neptune to expand its orbit from  $\sim 23$  to 30 AU, as seemingly demanded by the large observed population of resonant KBOs (C06), the planet must scatter at least  $\sim 7/30 \sim 25\%$  of its own mass in planetesimals, or about  $4M_\oplus$ . Spreading such a mass over a disk of radius 30 AU yields a surface density on the order of  $0.03 \text{ g/cm}^2$ , which falls within the range of  $\sigma$ 's that we find characterize instability. Clean-up and migration go hand-in-hand.

The disk masses that we found to be relevant for instability are smaller than the masses in the planets. This raises concern about the validity of our approximation that disk properties remain fixed throughout the simulation. One way of testing this approximation is to compare the change in the total angular momentum of all planets (brought about by dynamical friction) to the angular momentum available in the disk. If the former were much larger than the latter, then our neglect of back-reaction upon the disk would be a poor assumption. For the simulations displayed in Figs. 10 and 13, we find that the change in the  $z$ -component of angular momentum of all planets (including ejected ones) is nearly identical to the angular momentum available in the disk, indicating that our assumption of a fixed disk may be only marginally valid. (An analogous test for the energy would be inconclusive since the disk is supposed to be a sink of energy by virtue of dissipative collisions). For ideas on how to treat planet-disk interactions self-consistently, see Lithwick & Chiang (2007) and Levison & Morbidelli (2007).

##### 4.2.3. Disk Optical Depths and Comparison to Debris Disks

A planetesimal disk of surface density  $\sigma$  has a geometric vertical optical depth  $\tau_p \sim 4 \times 10^{-6} [\sigma / (0.01 \text{ g/cm}^2)] (10 \text{ m/p})$ , where  $p$  is the assumed planetesimal radius. Collisions between planetesimals, which occur over a timescale  $\sim 1 / (\Omega \tau_p) \sim 10^7$  yr at 30 AU, generate smaller dust particles whose optical depth is orders of magnitude higher. For example, if the dust size distribution obeys a Dohnanyi (1969) spectrum, then the geometric, vertical optical depth in  $s$ -sized grains would be  $\tau_d \sim \tau_p (p/s)^{1/2} \sim 0.01 [\sigma / (0.01 \text{ g/cm}^2)] (10 \text{ m/p})^{1/2} (\mu\text{m/s})^{1/2}$ . This is comparable to the vertical optical depths of some of the brightest extra-solar debris disks observed, e.g.,  $\beta$  Pic (Artymowicz 1997), HR 4796A (Li & Lunine 2003), and AU Mic (Strubbe & Chiang 2006), systems that are all  $\sim 10^7$  yr old. The observed paucity of stars with optically thicker disks implies that large populations of planetesimals having sizes  $p < 10 \text{ m}$  at stellocentric distances of  $\sim 30$  AU cannot be maintained for longer than  $\sim 10^7$  yr. The surface density in such collisional objects must be reduced by at least 2 orders of magnitude below planet-forming values of  $\sim 1 \text{ g/cm}^2$  within this timescale. In other words, planetesimals that are both collisional and planet-forming, like the kind espoused by GLS04, must be cleaned up fairly quickly.

#### 4.2.4. Instability in Our Solar System and Others

We have demonstrated that more than 2 ice giants may once have orbited the Sun. The current architecture of the outer solar system may well have resulted from a prior era of dynamical instability during which Uranus, Neptune, and 1 or 2 other ice giants crossed paths.

We expect similar instabilities to afflict all nascent planetary systems. Perhaps planet-planet instabilities are reflected in the large orbital eccentricities exhibited by most extra-solar gas giants (Marzari & Weidenschilling 2002; Ford et al. 2003; but for an alternative view see Goldreich & Sari 2003). The case of Upsilon Andromedae fits this picture (Ford et al. 2005). The difference between our solar system and systems like Upsilon Andromedae might be the surface density of the parent disk at the time of the last planet-planet scattering (Ford 2006). The time of last scattering will vary widely because of the chaotic nature of multi-planet systems. In the case of the solar system, the disk surface density must have been large enough at the time of last scattering for dynamical friction to damp the eccentricities and inclinations of surviving planets back down.

Viscous stirring rates vary with the semi-major axis separation between oligarchs. At least in the case without gas giants, the time for oligarchs to undergo close encounters increases by several orders of magnitude as their semi-major axis spacing is increased from 3 to 7 mutual Hill radii (Chambers et al. 1996). The disk surface density required for instability depends directly on this time, i.e.,  $\sigma_{\text{crit}} \propto 1/t_{\text{unstable}}$  in our eqn. (18). Whether  $t_{\text{unstable}}$  varies as strongly with oligarch spacing when perturbations by Jupiter and Saturn are included is not known, but preliminary experiments by us suggest that it does not. When we change the oligarch spacing from our standard 5 Hill radii to 3 Hill radii in runs that include Jupiter, Saturn, and  $N_{\text{olig}} = 5$  oligarchs, we find that the probability of 1 ejection still peaks at  $\sim 50\%$  for  $\sigma/\Sigma \approx 0.1$  (accounting for the factor of 2 increase in  $\Sigma$  due to the shorter spacing).

#### 4.2.5. Evidence for the Velocity Instability in the Kuiper Belt

Did velocity-unstable ice giants excite the large eccentricities and inclinations of the scattered Kuiper belt, as proposed by C06? Our provisional answer is no, as we

were unable to reproduce the large inclinations of scattered KBOs. For runs with disk surface densities down to  $\sim 0.01 \text{ g/cm}^2$ , oligarchs spend too little time, less than  $\sim 10^7 \text{ yr}$ , passing through the Kuiper belt. Moreover, oligarchs in our simulations have orbital inclinations that rarely exceed  $10^\circ$ .

To remedy the situation, we might appeal to still lower disk surface densities, on the order of  $\sim 0.001 \text{ g/cm}^2$ , for which dynamical friction cooling times for embedded planets would be as long as  $\sim 10^8 \text{ yr}$ . We found this region of parameter space difficult to explore. Out of 100 simulations starting with (a)  $N_{\text{olig}} = 4$ , (b) our compact set of initial conditions, and (c)  $\sigma = 0.002 \text{ g/cm}^2$ , only 6 yielded systems each with 2 surviving oligarchs at the end of the integrations at  $t = 10^8 \text{ yr}$ . Unfortunately, 5 of these 6 systems had not stabilized, and it was unclear whether more oligarchs would be ejected were the integrations to continue. Furthermore, over these long timescales, effects resulting from time variations in  $\sigma$  (see §4.2.2) might be expected to be important, and we have not modeled these.

Cooling times for planets and, by extension, KBO heating times might also be prolonged in more realistic treatments of dynamical friction that incorporate non-axisymmetries and the clearing of gaps in the disk. Ways of numerically simulating the response of planetesimal disks to planets can be found in Levison & Morbidelli (2007) and Lithwick & Chiang (2007).

We thank Ben Collins, Yoram Lithwick, Ruth Murray-Clay, Re'em Sari, and an anonymous referee for helpful exchanges. We also thank Harold Levison and Alessandro Morbidelli for generously sharing some of their ideas about planet-disk interactions and suggesting that we examine the angular momentum and energy budgets of our simulations. Support for E.B.F. was provided by a Miller Research Fellowship and by NASA through Hubble Fellowship grant HST-HF-01195.01A awarded by the Space Telescope Science Institute, which is operated by the Association of Universities for Research in Astronomy, Inc., for NASA, under contract NAS 5-26555. E.C. acknowledges grants from the National Science Foundation (AST-0507805), NASA (JPL-1264475), and the Alfred P. Sloan Foundation.

## REFERENCES

Artymowicz, P. 1997, Annual Review of Earth and Planetary Sciences, 25, 175

Binney, J., & Tremaine, S. 1987, *Galactic Dynamics* (Princeton: Princeton University Press), 424

Butler, R.P., et al. 2006, ApJ, 646, 505

Chambers, J.E. 2006, Icarus, 180, 496

Chambers, J.E. 1999, MNRAS, 304, 793

Chambers, J.E., Wetherill, G.W., & Boss, A.P. 1996, Icarus, 119, 261

Chiang, E.I., & Lithwick, Y. 2005, ApJ, 628, 520

Chiang, E.I., et al. 2006, in *Protostars and Planets V*, eds. B. Reipurth, D. Jewitt, & K. Keil (Tucson: Univ. Arizona Press), in press (astro-ph/0601654) (C06)

Collins, B.F., & Sari, R. 2006, AJ, 132, 1316

Collins, B.F., Schlichting, H.E., & Sari, R. 2007, AJ, in press

Dohnanyi, J.W. 1969, JGR, 74, 2531

Elliot, J.L., et al. 2005, AJ, 129, 1117

Ford, E.B. 2006, in *New Horizons in Astronomy: Frank N. Bash Symposium*, ASP Conference Series Vol. 352 (San Francisco: Astronomical Society of the Pacific), 15

Ford, E.B., Lystad, V., & Rasio, F.A. 2005, Nature, 434, 873

Ford, E.B., Rasio, F.A., & Yu, K. 2003, in *Scientific Frontiers in Research on Extrasolar Planets*, ASP Conference Series Vol. 294, eds. D. Deming & S. Seager (San Francisco: Astronomical Society of the Pacific), 181

Goldreich, P., Lithwick, Y., & Sari, R. 2004, ARA&A, 42, 549 (GLS04)

Goldreich, P., & Sari, R. 2003, ApJ, 585, 1024

Goldreich, P., & Tremaine, S. 1982, ARA&A, 20, 249

Greenberg, R., et al. 1991, Icarus, 94, 98

Ida, S., & Makino, J. 1993, Icarus, 106, 210

Kenyon, S.J., & Luu, J.X. 1999, 118, 1101

Levison, H.F., & Stewart, G.R. 2001, Icarus, 153, 224

Levison, H.F., et al. 2006, in *Protostars and Planets V*, eds. B. Reipurth, D. Jewitt, & K. Keil (Tucson: Univ. Arizona Press), in press

Levison, H.F., & Morbidelli, A. 2007, Icarus, in press

Li, A., & Lunine, J. I. 2003, ApJ, 590, 368

Lissauer, J.J., Pollack, J.B., Wetherill, G.W., & Stevenson, D.J. 1995, in *Neptune and Triton*, ed. D. Cruikshank (Tucson: Univ. Arizona Press), 37

Lithwick, Y., & Chiang, E. 2007, ApJ, in press (astro-ph:0607241)

Marzari, F., & Weidenschilling, S.J. 2002, Icarus, 156, 570

Matsuyama, I., Johnstone, D., & Hartmann, L. 2003, ApJ, 582, 893

Murray-Clay, R.A., & Chiang, E.I. 2006, ApJ, 651, 1194

Rafikov, R.R. 2004, AJ, 128, 1348

Shu, F.H., Johnstone, D., Hollenbach, D. 1993, Icarus, 106, 92

Stewart, G.R., & Ida, S. 2000, Icarus, 143, 28

Strubbe, L.E., & Chiang, E.I. 2006, ApJ, 648, 652

Thommes, E.W., Duncan, M.J., & Levison, H.F. 1999, Nature, 402, 635

Thommes, E.W., Duncan, M.J., & Levison, H.F. 2002, AJ, 123, 2862

Tsiganis, K., et al. 2005, Nature, 435, 459

Wisdom, J., & Holman, M. 1991, AJ, 102, 1528

Youdin, A.N., & Chiang, E.I. 2004, ApJ, 601, 1109

Youdin, A.N., & Shu, F.H. 2002, ApJ, 580, 494